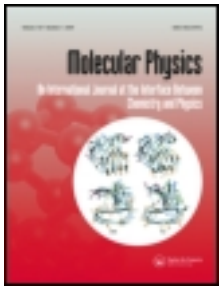

Molecular Physics: An International Journal at the Interface Between Chemistry and Physics
Publication details, including instructions for authors and subscription information:
http://www.tandfonline.com/loi/tmph20

Electric-field-induced inelastic collisions between magnetically trapped hydroxyl radicals

Benjamin K. Stuhl [a b], Mark Yeo [a b], Matthew T. Hummon [a b] & Jun Ye [a b]
[a] JILA, National Institute of Standards and Technology and University of Colorado, Boulder, CO, USA
[b] Department of Physics, University of Colorado, Boulder, CO, USA
Published online: 13 Jun 2013.

To cite this article: Benjamin K. Stuhl, Mark Yeo, Matthew T. Hummon & Jun Ye (2013) Electric-field-induced inelastic collisions between magnetically trapped hydroxyl radicals, Molecular Physics: An International Journal at the Interface Between Chemistry and Physics, 111:12-13, 1798-1804, DOI: 10.1080/00268976.2013.793838

To link to this article: http://dx.doi.org/10.1080/00268976.2013.793838

Molecular Physics, 2013
Vol. 111, Nos. 12–13, 1798–1804, http://dx.doi.org/10.1080/00268976.2013.793838

INVITED ARTICLE

Electric-field-induced inelastic collisions between magnetically trapped hydroxyl radicals

Benjamin K. Stuhl[a,b,†], Mark Yeo[a,b], Matthew T. Hummon[a,b] and Jun Ye[a,b,*]

[a]*JILA, National Institute of Standards and Technology and University of Colorado, Boulder, CO, USA;* [b]*Department of Physics, University of Colorado, Boulder, CO, USA*

(*Received 29 January 2013; final version received 29 March 2013*)

Inelastic collisions are observed between magnetically trapped neutral hydroxyl ($OH^{\bullet}$) radicals at a temperature of 45 mK in the presence of an electric field. The collision rate is measured over a range of electric fields from 0.2 to 10 kV/cm. However, the two-body collision rates must be deconvolved from a novel electric-field induced non-adiabatic single particle loss, which arises from Landau–Zener crossings between energy surfaces at the plane where the electric field vector is transverse to the trapping magnetic field. The observed inelastic collision rate follows an approximate quadratic power law in the effective dipole moment.

Keywords: inelastic collisions; hydroxyl (OH) radicals; cold molecules; non-adiabatic trap loss;

Cold molecular collisions constitute a unique nexus between chemical theory and experiment. The reduction in computational complexity due to the limited set of energetically allowed channels and partial waves enables the use of cutting-edge scattering codes to directly study the interactions at a true *ab initio* level [1]. In conjunction, the explosive growth of cold molecule techniques over the past decade – particularly association of ultracold atoms [2], Stark [3–6] or Zeeman [7,8] deceleration, buffer-gas cooling [9–13], and assorted guiding methods [14,15] – is now beginning to allow experimental tests [15–18] of these calculations.

One molecule in particular stands out for its broad interest across many disciplines: the hydroxyl ($OH^{\bullet}$) radical. Hydroxyl is at the heart of combustion reactions [19–24] and of atmospheric chemistry [25–27]; it is even found at cosmological distances in other galaxies [28,29]. While OH–OH reactions are rare in the atmosphere, due to hydroxyl's low abundance, the reactions

$$OH + OH \rightarrow O(^3P) + H_2O \quad (1)$$

$$OH + OH + M \rightarrow H_2O_2 + M \quad (2)$$

are both of great importance to combustion. Both reactions terminate a reaction chain in the forward direction, while reaction (1) creates the pseudo-equilibrium found in post-flame combustion conditions [30]. Hydroxyl molecules have been both magnetically [16,31] and electrostatically [32] trapped at temperatures of 50–500 mK. Recently, evaporative cooling was observed in magnetically trapped OH molecules [5], which opens the door to the creation of sub-millikelvin temperatures and observation of true *s*-wave dominated collisions and chemical reactions of this important molecule[1]. In this paper, we report an observation of OH–OH inelastic collisions at 45 mK, resulting in two-body losses from a magnetic quadrupole trap. The observed collision rates are substantially *tunable* through the application of a static electric field, although substantial theoretical work may be needed to determine whether that is due to true dipolar interactions or modifications of the scattering potential by electric-field-induced mixing of opposite-parity states. These inelastic collision results provide both a benchmark for calculations and a potential guide towards improved evaporation efficiency.

Cooling and magnetic trapping of state-selected OH molecules follows a procedure described elsewhere [5,16,31,33–37]. The OH radicals are created by a pulsed electric discharge through a supersonic expansion of saturated water vapour in 1.5 bar of a krypton carrier gas, yielding a gas packet with a comoving temperature of several Kelvin and a mean forward velocity of ∼500 m/s. The packet is $\gtrsim$95 % in the $v = 0$ vibrational ground state and, due to the large rotational constant and spin-orbit constants of OH, is almost purely in the $X^2\Pi_{3/2}$, $J = 3/2$ rotational ground state. J denotes the total angular momentum quantum number excluding nuclear spin, with laboratory projection M and projection Ω on the internuclear axis of the molecule.

[†]Present address: Joint Quantum Institute, National Institute of Standards and Technology, Gaithersburg, Maryland 20899, USA
[*]Corresponding author. Email: ye@jila.colorado.edu

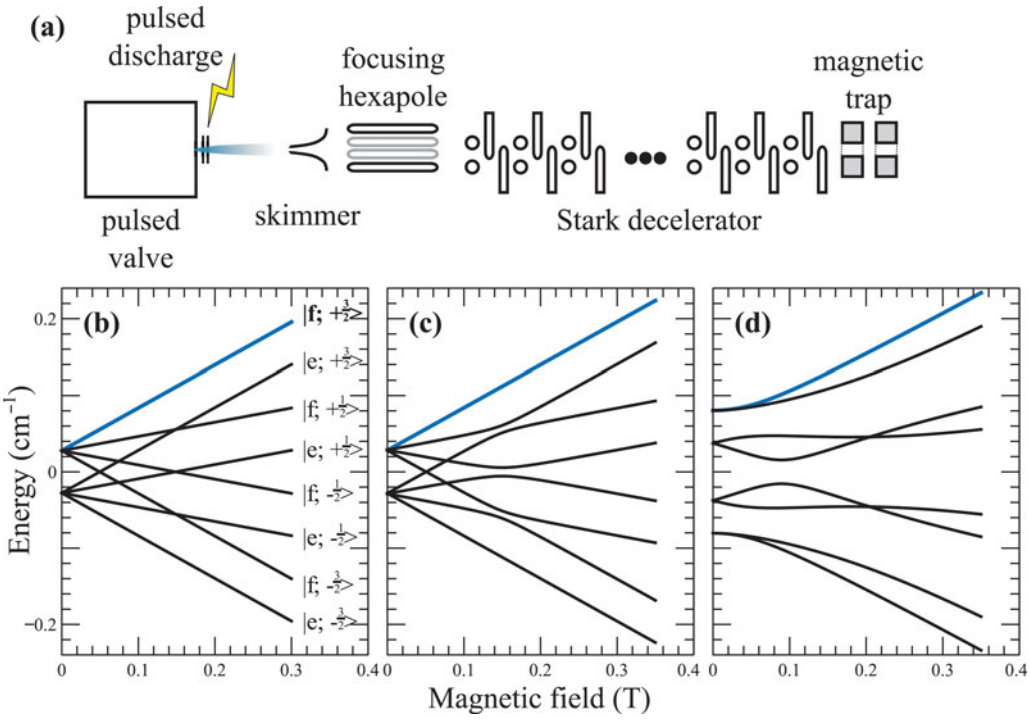

Figure 1. (a) A schematic drawing of the Stark decelerator and magnetic trapping system. The magnets, which create the magnetic trap potential (far right), are also used as the final stage of the Stark decelerator, so that molecules are loaded into the trap with zero center-of-mass velocity. (b)–(d) Calculated Zeeman spectra of $X^2\Pi_{3/2}$, $v = 0$, $J = 3/2$ ground-state OH in the presence of orthogonal electric fields of various strengths: (b) 0 V/cm, (c) 500 V/cm and (d) 5000 V/cm. The magnetic trap is loaded with molecules in the blue, uppermost $|f; M = +3/2\rangle$ adiabatic state.

The fast-moving packet is collimated by a skimmer and then focused by an electrostatic hexapole into the entrance of a Stark decelerator [31,38], as shown in Figure 1(a). The Stark decelerator uses pulsed electrostatic fields to conservatively slow a fraction of the initial packet down to 34 m/s at its output. Since the decelerator is only effective on molecules in the electric weak-field-seeking parity state, the slowed packet is further state-purified to a single parity state and only two Zeeman sublevels $M = \pm 3/2$. The slowed packet then flies into the magnetic quadrupole trap formed by a pair of anti-Helmholtz ring-geometry permanent magnets, with 4 mm inner diameter, 12 mm outer diameter and 4 mm thickness. The molecules are stopped at the trap center by an electric field of 61 kV/cm, created by charging the surface plating of the magnets. At the instant the mean molecular velocity is brought to zero, the electric field is turned off, leaving the half of the slowed packet in the $M = +3/2$ sublevel confined by the magnetic trap, while the $M = -3/2$ molecules escape in less than 1 ms. Once trapped, in the absence of any electric fields the molecules are stably confined for time scales of $\sim$1 s, limited by the vacuum quality of the trap chamber. Molecules are detected by state-sensitive laser-induced fluorescence (LIF), which uses pulsed-laser excitation on the $A^2\Sigma(v = 1) \leftarrow X^2\Pi_{3/2}(v = 0)$ transition at 282 nm to produce Stokes-shifted fluorescence on the $A^2\Sigma(v = 1) \rightarrow X^2\Pi_{3/2}(v = 1)$ line at 313 nm. Unfortunately, pulsed-laser LIF has large systematic uncertainties and therefore provides only a relative measurement of the number of molecules illuminated rather than an absolute measurement of trap population.

In its ground state, hydroxyl is not perfectly described by either Hund's case *a* or case *b* couplings, since its rotational splitting $BJ(J + 1) \gtrsim 70.9$ cm^{-1} and spin-orbit constant $A = -139.2$ cm^{-1} [39] are of similar orders (the negative sign in A denotes that the $\Omega = 3/2$ manifold is lower in energy than the $\Omega = 1/2$ manifold). However, Hund's case *a* treatment is a reasonable approximation for the specific case of the lowest J state within each manifold. Therefore, we describe OH using a $|JM\Omega\epsilon\rangle$ basis, where J, M and Ω have already been defined and $\epsilon = e$ or f denotes the J-relative parity eigenstate of the molecule. Electric (E) fields mix states of opposite parity; however, the $|e\rangle$ and $|f\rangle$ states are split by a Λ-doubling interaction of 1667 MHz and therefore the electric strong- and weak-field-seeking states can be adiabatically tracked to the $|e\rangle$ or $|f\rangle$ parity labels, respectively.

In the absence of an electric field, the Zeeman spectrum of ground-state OH is purely linear, as shown in Figure 1(b), with a molecule-fixed magnetic moment of

$\mu_{\text{bare}} = 2\mu_B$, where μ_B is the Bohr magneton. In the laboratory frame, the body-fixed moment is rotationally averaged to yield an effective moment

$$\mu_{\text{eff}} = \frac{M\Omega}{J(J+1)}\mu_{\text{bare}}; \tag{3}$$

the same rotational averaging applies to the molecule-fixed electric dipole moment of 1.67 D. Since the electric dipole interaction $-\vec{E}\cdot\vec{\mu}$ couples states of opposite parity and $\Delta M = \pm 1$ or 0, electric fields cause the Zeeman crossings between opposite parity states to acquire an energy gap and become increasingly avoided [40,41]. Figure 1(c) and (d) demonstrate this effect with two different electric field strengths: at electric fields $\gtrsim$2 kV/cm, the molecule is effectively fully polarised at zero magnetic field (B), and so the low-B spectrum is dominated by the electric-field-induced avoided crossings. However, the magnetic trap is loaded with molecules purely in the uppermost $|f; M = +3/2\rangle$ adiabatic state – which is magnetically weak-field-seeking for arbitrary electric and magnetic field combinations, and so these molecules always see a confining potential.

Since the molecules are trapped at a temperature of 45 mK, collisional excitation to higher rotational or vibrational states is thermodynamically impossible. Inelastic collisions nonetheless can cause trap losses in several other ways. The first possibility is a simple M-changing collision, which transfers one or both collision partners into an untrapped lower-M state. The second possibility is slightly more subtle: while the $|e; M = +3/2\rangle$ state is magnetically trapped (at least in the absence of electric fields [41]), it is nonetheless dark to LIF because the parity selection rule requires that the $|e\rangle$ and $|f\rangle$ states be excited to different, spectroscopically resolved rotational levels in the $A^2\Sigma$ manifold. Therefore, parity-changing $|f\rangle$-to-$|e\rangle$ collisions also appear as trap loss. While it is expected that the rates of reactive collisions are much lower than those of inelastic state-changing collisions, the third and most exciting possibility is chemical reactions through mechanism (1).

In the absence of electric fields, we observe no sign of inelastic collisions after a trap settling time of ~10 ms: measurements of fluorescence versus time are consistent with pure one-body loss due to scattering by background gas for time scales as long as 1 s. However, the application of a static electric field (created by applying voltages to the trap magnets) causes the loss of molecules with a two-body loss time profile. If molecules are lost with a one-body loss rate Γ and a homogeneous two-body coefficient β according to

$$\frac{dN}{dt} = -\Gamma N - \beta N^2, \tag{4}$$

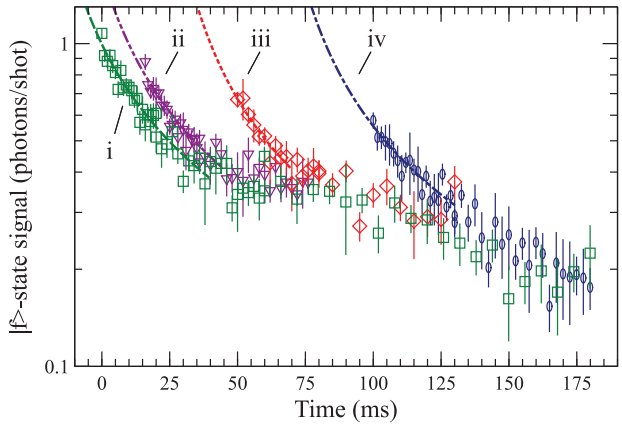

Figure 2. Fluorescence versus time graphs, showing the two-body character of the observed trap loss. An electric field of 3,040 V/cm was turned on synchronously with the first point of each curve; the different delays before the turn-on of the electric field allow the initial OH density to vary by a factor of two between curves (i) and (iv). Curves demonstrate pure two-body-loss fits, with rate parameters of (i) 40.4 ± 3.0 (photons/shot)$^{-1}$s^{-1} (IPSS), (ii) 41.2 ± 4.2 IPSS, (iii) 48.4 ± 8.1 IPSS and (iv) 45.4 ± 5.5 IPSS. Error bars are one standard error.

then the number-versus-time curve $N(t)$ obeys

$$N(t) = \frac{\Gamma N_0}{(\Gamma + \beta N_0)\, e^{\Gamma t} - \beta N_0}, \tag{5}$$

where $N_0 = N(t = 0)$ is the initial number of molecules. To disentangle one- and two-body losses, it is rarely sufficient to fit data to the form of Equation (5), unless multiple decades of dynamic range are available. Since our typical results do not have that much range, we instead varied the initial number of molecules (i.e. the initial density) and confirmed that the loss rates are density dependent and also yield consistent measurements of the two-body parameter β. Figure 2 shows typical results from this programme: the initial density was varied by allowing one-body loss to homogeneously reduce the trap density before turning on the electric field to initiate two-body losses. All four curves in Figure 2 were taken using the same electric field of 3040 V/cm; the field was turned on at the first point in each different curve. While the initial density and the initial semi-logarithmic slopes both vary by a factor of two, all four curves yield consistent values for β. (For conceptual clarity, the fits shown in Figure 2 omit the one-body term, since it is small and identical for all four data-sets; explicit accounting of the one-body losses does not qualitatively change the fits.) Since LIF does not provide an absolute scale for the density, all measurements are quoted using units of fluorescence photons per realisation of the experiment, which is proportional to the number of molecules. Each point in Figure 2 is an average of ~1500 realisations.

To determine the electric-field dependence of the inelastic collisions, we repeated the experiment using many

different values of the electric field, over a range of 0.2–10 kV/cm. Since the $|e\rangle$ and $|f\rangle$ parity states are split by Λ-doubling, at electric fields below the polarising field $E_{\mathrm{pol}} \approx 2$ kV/cm OH has a quadratic Stark shift and therefore an electric-field-dependent dipole moment in the laboratory frame. The effective moment $d_{\mathrm{eff}}(E)$ is given by

$$d_{\mathrm{eff}} = \frac{d_{\mathrm{polarised}}^2 \cdot E}{\sqrt{\left(\frac{\Delta}{2}\right)^2 + \left(d_{\mathrm{polarised}} \cdot E\right)^2}}, \tag{6}$$

where $d_{\mathrm{polarised}} = 1.002$ D is the full rotationally averaged moment and $\Delta = 1667.4$ MHz is the Λ-doublet splitting. Our range of electric fields therefore covers both the quadratic regime where d_{eff} varies and the polarised regime where $d_{\mathrm{eff}} \approx d_{\mathrm{polarised}}$ is approximately independent of electric field.

There exists one substantial complication to accurately determining the two-body rate as a function of electric field, which is that the one-body rate also varies with electric field. This variation is due to a mechanism reminiscent of Majorana loss, resulting from Landau–Zener crossings caused by a combination of small magnetic fields and large transverse electric fields, as described in Appendix A. However, since the trapped molecules are observed to be in thermal equilibrium [5], the one-body loss rates are amenable to simple numeric integral calculations. At small electric fields, the losses are negligible: at 2 kV/cm, the rate is only 1 s^{-1}. However, the rate rises very rapidly with increasing electric field and reaches 50 s^{-1} at 10 kV/cm – much faster than the vacuum losses and therefore an effect which must be accounted for.

With the one-body losses deconvolved from the experimental data, the true two-body loss coefficient β can be determined. Figure 3(a) plots β as a function of electric field. Figure 3(b) additionally displays the effective dipole moment for each electric field value. Error bars on the data points are statistical; the shaded region shows the range of values generated by halving or doubling the calculated one-body rates. While the true systematic uncertainty in the one-body calculations is not known, β does not depend strongly on their accuracy.

There are several observations, which can be made about the two-body loss rates even in the absence of theoretical scattering calculations. The first is that the rates are too small to observe against one-body loss rates of 2–5 s^{-1} below fields of ∼600 V/cm. A second point is that there is a clear dependence of the loss rate on the induced dipole moment, although it is different from the $\beta \propto d_{\mathrm{eff}}^6$ power law observed in inelastic p-wave dominated scattering of ultracold fermionic KRb [42,43]. It is known, however, that electric fields will generically lower the long-range repulsive barrier between state-selected $|f; +3/2\rangle$ molecules [5] A third point applies to the behaviour of the loss rate as the dipole moment saturates. It can be seen in Figure 3 that the central value of β continues to increase with electric field, even as the dipole moment starts to saturate; however, a factor-of-two increase in the assumed one-body rate (the lower limit of the shaded region) is sufficient to make the apparent two-body rate saturate along with the dipole moment. Further increases in the assumed one-body rate cause the fitted inelastic rate to acquire a non-monotonic dependance on the electric field, which seems unlikely and therefore sets an upper bound on the uncertainty of the one-body rate.

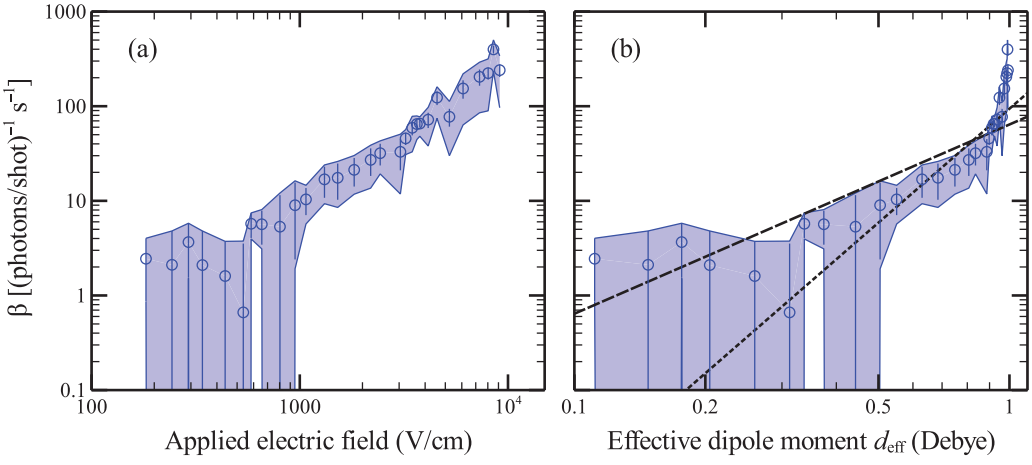

Figure 3. Two-body loss rate coefficients as a function of (a) electric field and (b) effective dipole moment. The rates have been fitted using a combined one- and two-body loss form, incorporating both vacuum-scattering and non-adiabatic losses in the one-body term. The shaded region illustrates the variation in the determined two-body rate if the calculated non-adiabatic rate is assumed to over- or under-estimate the true loss rate by a factor of two; this constitutes a global rather than point-by-point systematic uncertainty. Each point is a weighted mean of multiple measurements using different initial densities; error bars are one weighted statistical standard error. The dashed and dotted lines of (b) are guides to the eye, demonstrating d_{eff}^2 and d_{eff}^4 power-laws, respectively.

In summary, electric-field-induced inelastic collisions have been observed between magnetically trapped hydroxyl radicals at a temperature of 45 mK. Determination of the true inelastic rate required characterisation of a novel form of non-adiabatic trap loss, induced by the application of transverse electric fields. The availability of this low-temperature and few-partial-wave scattering data should provide a strong constraint for future theoretical studies of the long-range OH–OH interaction potentials.

Acknowledgements

We thank G. Quéméner and J. L. Bohn for stimulating discussions. We acknowledge funding from the NSF Physics Frontier Center, NIST, DOE, and the AFOSR and ARO MURIs on Cold Molecules.

Note

1. The *s*-wave cross-section enters the threshold regime around 200 μK.

References

[1] G. Quéméner and P.S. Julienne, Chem. Rev. **112**, 4949 (2012).
[2] K.K. Ni, S. Ospelkaus, M.H.G. de Miranda, A. Pe'er, B. Neyenhuis, J.J. Zirbel, S. Kotochigova, P.S. Julienne, D.S. Jin, and J. Ye, Science **322**(5899), 231 (2008).
[3] H.L. Bethlem, G. Berden, and G. Meijer, Phys. Rev. Lett. **83**(8), 1558 (1999).
[4] J.R. Bochinski, E.R. Hudson, H.J. Lewandowski, G. Meijer, and J. Ye, Phys. Rev. Lett. **91**(24), 243001 (2003).
[5] B.K. Stuhl, M. Yeo, M.T. Hummon, G. Quéméner, J. Bohn, and J.L. Ye, Nature **492**, 396 (2012).
[6] S.Y.T. van de Meerakker, H.L. Bethlem, N. Vanhaecke, and G. Meijer, Chem. Rev. **112**(9), 4828 (2012).
[7] E. Narevicius, A. Libson, C.G. Parthey, I. Chavez, J. Narevicius, U. Even, and M.G. Raizen, Phys. Rev. A **77**(5), 051401 (2008).
[8] E. Narevicius and M.G. Raizen, Chem. Rev. **112**(9), 4879 (2012).
[9] B. Friedrich, J.D. Weinstein, R. deCarvalho, and J.M. Doyle, J. Chem. Phys. **110**(5), 2376 (1998).
[10] D. Egorov, T. Lahaye, W. Schöllkopf, B. Friedrich, and J.M. Doyle, Phys. Rev. A **66**(4), 043401 (2002).
[11] L.D. van Buuren, C. Sommer, M. Motsch, S. Pohle, M. Schenk, J. Bayerl, P.W.H. Pinkse, and G. Rempe, Phys. Rev. Lett. **102**, 033001 (2009).
[12] S.M. Skoff, R.J. Hendricks, C.D.J. Sinclair, J.J. Hudson, D.M. Segal, B.E. Sauer, E.A. Hinds, and M.R. Tarbutt, Phys. Rev. A **83**, 023418 (2011).
[13] N.R. Hutzler, H.I. Lu, and J.M. Doyle, Chem. Rev. **112**(9), 4803 (2012).
[14] C. Sommer, M. Motsch, S. Chervenkov, L.D. van Buuren, M. Zeppenfeld, P.W.H. Pinkse, and G. Rempe, Phys. Rev. A **82**, 013410 (2010).
[15] A.B. Henson, S. Gersten, Y. Shagam, J. Narevicius, and E. Narevicius, Science **338**, 234 (2012).
[16] B.C. Sawyer, B.K. Stuhl, D. Wang, M. Yeo, and J. Ye, Phys. Rev. Lett. **101**(20), 203203 (2008).
[17] M. Kirste, L. Scharfenberg, J. Kłos, F. Lique, M.H. Alexander, G. Meijer, and S.Y. van de Meerakker, Phys. Rev. **A 82**, 042717 (2010).
[18] T.V. Tscherbul, Z. Pavlovic, H.R. Sadeghpour, R. Côté, and A. Dalgarno, Phys. Rev. A **82**, 022704 (2010).
[19] F. Haber, Angew. Chem. **42**, 745 (1929).
[20] V.N. Kondrat'ev, Usp. Khim. **8**, 195 (1939).
[21] J. Warnatz, Combust. Sci. Technol. **34**, 177 (1983).
[22] C.K. Westbrook, Proc. Combust. Inst. **28**, 1563 (2000).
[23] J.A. Miller, M.J. Pilling, and J. Troe, Proc. Combust. Inst. **30**, 43 (2005).
[24] J.A. Miller, R.J. Kee and C.K. Westbrook, Ann. Rev. Phys. Chem. **41** 345 (1990).
[25] R. Atkinson, Chem. Rev. **86**, 69 (1986).
[26] B.J. Finlayson-Pitts and J.N. Pitts, Science **276**, 1045 (1997).
[27] J. Lelieveld, F.J. Dentener, W. Peters, and M.C. Krol, Atmos. Chem. Phys. **4**, 2337 (2004).
[28] K.Y. Lo, Ann. Rev. Astron. Astrophys. **43**, 625 (2005).
[29] K.W. Willett, J. Darling, H.W.W. Spoon, V. Charmandaris, and L. Armus, Astrophys. J. **730**(1), 56 (2011).
[30] M.K. Bahng and R.G. Macdonald, J. Phys. Chem. A **111**(19), 3850 (2007).
[31] B.C. Sawyer, B.L. Lev, E.R. Hudson, B.K. Stuhl, M. Lara, J.L. Bohn, and J. Ye, Phys. Rev. Lett. **98**(25), 253002 (2007).
[32] S.Y.T. van de Meerakker, P.H.M. Smeets, N. Vanhaecke, R.T. Jongma, and G. Meijer, Phys. Rev. Lett. **94**, 023004 (2005).
[33] J.R. Bochinski, E.R. Hudson, H.J. Lewandowski, and J. Ye, Phys. Rev. A **70**, 043410 (2004).
[34] B.C. Sawyer, B.K. Stuhl, B.L. Lev, J. Ye, and E.R. Hudson, Eur. Phys. J. D **48**(2), 197 (2008).
[35] B.C. Sawyer, B.K. Stuhl, M. Yeo, T.V. Tscherbul, M.T. Hummon, Y. Xia, J. Kłos, D. Patterson, J.M. Doyle, and J. Ye, Phys. Chem. Chem. Phys. **13**, 19059 (2011).
[36] B.C. Sawyer, Ph. D. thesis, University of Colorado, 2010.
[37] B.K. Stuhl, Ph. D. thesis, University of Colorado, 2012.
[38] E.R. Hudson, C. Ticknor, B.C. Sawyer, C.A. Taatjes, H.J. Lewandowski, J.R. Bochinski, J.L. Bohn, and J. Ye, Phys. Rev. A **73**(6), 063404 (2006).
[39] J. Maillard, J. Chauville, and A. Mantz, J. Mol. Spectrosc. **63**(1), 120 (1976).
[40] M. Lara, B.L. Lev, and J.L. Bohn, Phys. Rev. A **78**, 033433 (2008).
[41] B.K. Stuhl, M. Yeo, B.C. Sawyer, M.T. Hummon, and J. Ye, Phys. Rev. A **85**, 033427 (2012).
[42] K.K. Ni, S. Ospelkaus, D. Wang, G. Quemener, B. Neyenhuis, M.H.G. de Miranda, J.L. Bohn, J. Ye, and D.S. Jin, Nature **464**, 1324 (2010).
[43] Z. Idziaszek, G. Quéméner, J.L. Bohn, and P.S. Julienne, Phys. Rev. A **82**(2), 020703 (2010).
[44] G. Quéméner and J.L. Bohn, Mol. Phys. (2013).
[45] J.R. Rubbmark, M.M. Kash, M.G. Littman, and D. Kleppner, Phys. Rev. A **23**(6), 3107 (1981).

Appendix. Electric-field-induced one-body losses of $|f\rangle$-state molecules

An examination of the two highest potential surfaces of OH molecules in a uniform electric field $\vec{E}$ superimposed over a quadrupole magnetic field $\vec{B}$ (Figure A1) reveals a fascinating structure. At small values of $E = |\vec{E}|$, the surfaces are almost indistinguishable from a pure linear magnetic quadrupole with the electric field's only effect being a tiny dimple near zero $B = |\vec{B}|$. As E increases, the distortion at small B grows, forming a ridge along the line $\vec{B} \perp \vec{E}$. At large $E \gtrsim E_{\mathrm{pol}}$, along this ridge the Zeeman splitting changes from linear to quadratic, creating a very

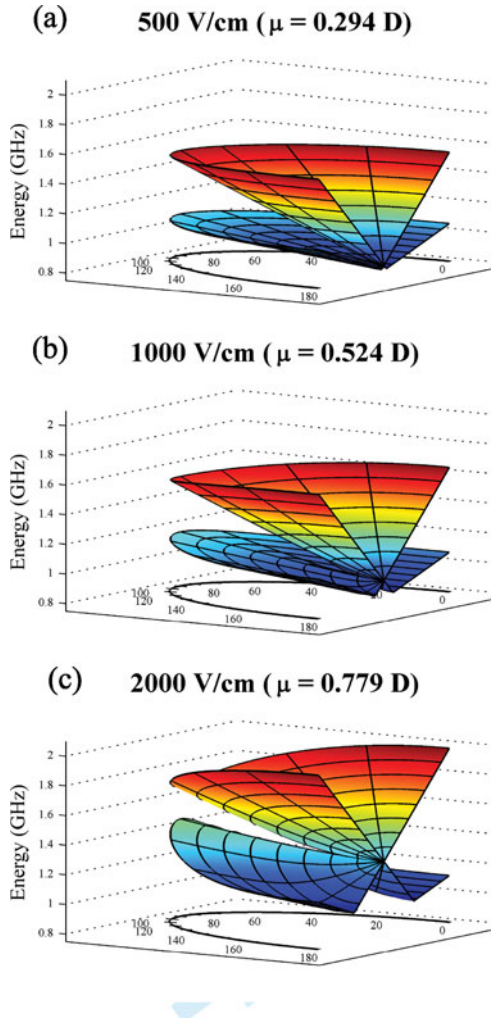

Figure A1. The two highest-energy adiabatic potential surfaces of ground-state OH in the presence of combined electric and magnetic fields. The radial coordinate is magnetic field, the azimuthal coordinate θ_{EB} is the angle between the electric and magnetic field vectors, and the vertical coordinate is the adiabatic energy of the state in GHz. Radial contours are spaced by 5 mT. Electric field strengths are (a) 500 V/cm, (b) 1000 V/cm and (c) 2000 V/cm. Other views of the potential surfaces, including three-dimensional fly-around movies, are available online as supplemental information.

narrow avoided crossing between the surfaces at small B. (An analytic discussion of the combined Stark-Zeeman Hamiltonian for Hund's case a molecules can be found in an article by Queménér and Bohn in this issue [44].)

This avoided crossing is the cause of the electric-field-dependent one-body losses. Just as relatively rapid changes in the direction of $\vec{B}$ can cause Majorana spin-flips in pure magnetic fields, in this crossed-field configuration small changes in the angle θ_{EB} between the electric and magnetic fields can allow molecules to make Landau–Zener crossings from the uppermost trapped state to the lower untrapped one. The transition probability is given by the Landau–Zener formula $P_{\mathrm{LZ}}(r) = e^{-2\pi G(r)}$ [45], where

$$G(\vec{r}) = \frac{\Delta\left(E,\ B(\vec{r}),\ \theta_{EB} = \frac{\pi}{2}\right)^2}{\hbar\left(d\Delta/d\theta_{EB}|_{\vec{r},\frac{\pi}{2}}\right)\left(d\theta_{EB}/dt|_{\vec{r},\frac{\pi}{2}}\right)} \tag{A1}$$

and $\Delta\left(E,\ B(\vec{r}),\ \theta_{EB}\right)$ is the splitting between the two surfaces at position $\vec{r}$. In the geometry of a homogeneous electric field superimposed over a three-dimensional quadrupole magnetic field, the only region of relevance is the 'disk of death', near the plane where $\theta_{EB} \approx \frac{\pi}{2}$. In this region, θ_{EB} is directly proportional to the polar angle ϑ about the direction of $\vec{E}$, and so taking the origin at the center of the quadrupole allows Equation (A1) to be greatly simplified to

$$G(r) = \frac{\Delta\left(E,\ B(r),\ \theta_{EB} = \frac{\pi}{2}\right)^2}{\hbar\left(d\Delta/d\theta_{EB}|_{r,\frac{\pi}{2}}\right)\left(\frac{1}{r}v_\vartheta\right)}, \tag{A2}$$

where v_ϑ is the molecule's velocity component in the $\hat{\vartheta}$ direction.

To determine an absolute loss rate Γ_{LZ}, it finally suffices to integrate the probability function P_{LZ} over the molecular Boltzmann distribution:

$$\Gamma_{\mathrm{LZ}} = \int_0^\infty 4\pi r^2 n_{\mathrm{r}}(r)\,dr \int_0^\infty \frac{1}{\pi}\frac{v_\vartheta}{r}\cdot e^{-2\pi G(r)}\cdot\frac{1}{Z}e^{-\frac{mv_\vartheta^2}{2k_BT}}\,dv_\vartheta,$$

where $n_{\mathrm{r}}(r)$ is the three-dimensional relative density with $\int_0^\infty 4\pi r^2 n_{\mathrm{r}}(r)\,dr = 1$, $Z = \int_0^\infty e^{-\frac{mv_\vartheta^2}{2k_BT}}\,dv_\vartheta$ is the velocity partition function, $m = 17$ amu is the molecular mass, k_B is Boltzmann's constant and T is the temperature. The factor $\frac{1}{\pi}\frac{v_\vartheta}{r}$ occurs because each molecule encounters $\theta_{EB} = \frac{\pi}{2} + n\pi$ twice per orbit. For a quadrupole magnetic trap of gradient B' in the $\hat{r}$ direction,

$$n_{\mathrm{r}}(r) = \frac{1}{Z_{\mathrm{n}}}e^{-\frac{\mu_m B' r}{k_B T}},$$

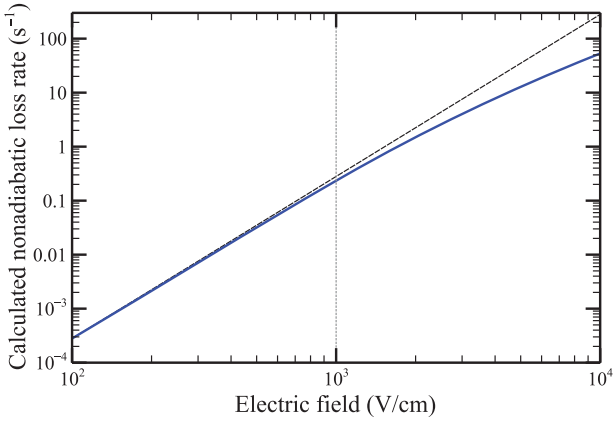

Figure A2. The calculated non-adiabatic loss rate as a function of applied electric field, for a 45 mK distribution confined within a linear quadrupole trap with a B-field gradient of 1 T/cm in the direction perpendicular to the electric field. The dashed line is a pure cubic power-law, matched to the calculated rate at 100 V/cm to provide a guide to the eye.

with

$$Z_{\mathrm{n}} = \int_0^\infty 4\pi r^2 e^{-\frac{\mu_m B' r}{k_B T}}\, dr$$

being the spatial partition function and μ_m being the magnetic moment of the molecule.

The resulting rate Γ_{LZ} can be found numerically, by diagonalising an 8×8 matrix in the $|JM\Omega\epsilon\rangle$ fine-structure plus parity basis [40,41] to calculate Δ and $d\Delta/d\theta_{EB}$ and then performing the Boltzmann integrals. For the specific case of our magnetic trap, with a 45 mK temperature and a 1 T/cm B-field gradient in the $\vec{E} \perp \vec{B}$ plane, the rate is plotted as a function of E in (Figure A2). It shows an approximately cubic dependence on E below E_{pol}, but shallows as the radius of the 'disk of death' becomes comparable to the trap radius.